FERMILAB-PUB-14-413-E

Scintillation Light from Cosmic-Ray Muons in Liquid Argon

D. Whittington[1] and S. Mufson[1]

[1] *Indiana University, Bloomington, Indiana 47405, USA*

(Dated: October 17, 2014)

This paper reports the results of the first experiment to directly measure the properties of the scintillation light generated by minimum ionizing cosmic-ray muons in liquid argon. Scintillation light from these muons is of value to studies of weakly-interacting particles in neutrino experiments and dark matter searches, as well as for particle identification. The experiment was carried out at the TallBo facility at Fermilab using prototype light guides and electronics developed for the Long-Baseline Neutrino Experiment. Analysis of the time-resolved structure of the scintillation light from cosmic-ray muons gives $\langle\tau_{\rm T}\rangle = 1.43 \pm 0.04$ (stat.) $\pm$ 0.007 (sys.) μs for the triplet light decay time constant. The ratio of singlet to triplet light measured using surface-coated light guides is $R = 0.39 \pm 0.01$ (stat.) ± 0.008 (sys.). There is some evidence that this value is not consistent with R for minimum ionizing electrons. However, the value for R measured here clearly differs significantly from R found for heavily ionizing particles like alphas. Furthermore, there is no apparent difference in R measured using light guides coated with TPB versus bis-MSB, adding additional evidence that bis-MSB is a promising alternative to TPB for detecting scintillation light in liquid argon.

PACS numbers: 13.85.Tp, 14.60.Ef, 29.40.Mc, 78.47.jd

I. INTRODUCTION

Liquid argon (LAr) is proving to be a sensitive and cost-effective detector medium for the study of weakly-interacting particles in neutrino experiments and dark matter searches. Signals generated in LAr by these particles' interactions include ionization electrons from charged daughter particles which can be detected directly by a time projection chamber or by photodetectors sensitive to the scintillation light from excited argon. In this paper we study the properties of the scintillation light generated by cosmic-ray muons in LAr using light collectors, photodetectors, and readout electronics being developed for the Long Baseline Neutrino Experiment (LBNE).

As charged particles pass through LAr, they create excited argon atoms that can pair with neutral argon atoms to form an excited argon dimer, which subsequently decays by emitting a scintillation photon. This process happens through two mechanisms:

$$\mathrm{Ar}^* + \mathrm{Ar} \rightarrow \mathrm{Ar}_2^* \rightarrow 2\mathrm{Ar} + \gamma \tag{1a}$$

$$\mathrm{Ar}^+ + \mathrm{Ar} \rightarrow \mathrm{Ar}_2^+,$$
$$\mathrm{Ar}_2^+ + e^- \rightarrow \mathrm{Ar}_2^* \rightarrow 2\mathrm{Ar} + \gamma. \tag{1b}$$

In both sequences the decay of the dimers result in an emission spectrum of vacuum ultraviolet (VUV) photons narrowly peaked at 128 nm.

The argon dimer can be excited to either a singlet ($^1\Sigma_u^+$) or triplet ($^3\Sigma_u^+$) state; the scintillation photons from these two states cannot be easily distinguished from one another spectroscopically. The mean lifetime of the singlet $^1\Sigma_u^+$ state is $\tau_{\rm S} \approx 6$ ns (early light); the triplet $^3\Sigma_u^+$ state is significantly longer-lived, with $\tau_{\rm T} \approx 1.4$ μs (late light) [1, 2]. The primary objectives of this investigation are to make a precision measurement of $\tau_{\rm T}$ for minimum ionizing cosmic-ray muons and to characterize the relative fraction of early light to late light that they produce.

Detecting the VUV scintillation photons from LAr in large neutrino detectors like LBNE is technically challenging because of the difficulty in detecting the VUV photons efficiently. Since significant photocathode coverage of the detector is prohibitively expensive, the scintillation photons are gathered by light guides that collect them, waveshift them into the optical, and then channel them to optical photodetectors. This detection scheme is inherently inefficient, but can be mitigated by two factors. First, LAr is a copious source of scintillation light, producing tens of thousands of VUV photons per MeV along a track [3]. Second, pure liquid argon is transparent to its own scintillation light, meaning the scintillation signal can be detected at a significant distance from its source. Many designs for the LBNE light guides are currently being evaluated. This investigation uses four prototype light guide designs for the measurements.

Scintillation light can prove to be useful in the analysis of experimental data in many ways. For experiments based on a time-projection chamber, the leading edge of the light pulse from the singlet decay provides sub-mm accuracy in the reconstruction of the absolute position of the event along the drift coordinate. For underground neutrino detectors, scintillation light can act as a supernova trigger. For both neutrino and dark matter experiments, scintillation light is useful for particle identification. Highly ionizing particles create a higher local density of electrons than minimum ionizing muons. This in turn induces more singlet decays, which lead to a larger fraction of light from singlet decays than triplet decays for highly ionizing particles. Further, for underground neutrino experiments the fraction of early to late light (pulse shape discrimination) contributes to the rejection of cosmic-ray spallation backgrounds. For a surface de-

Operated by Fermi Research Alliance, LLC under Contract No. De-AC02-07CH11359 with the United States Department of Energy.

tector this ratio provides information useful to algorithms that reject background cosmic rays [4].

Minimum ionizing cosmic-ray muons are expected to behave like minimum ionizing electrons in LAr. Here we report the first direct measurements of the muon's scintillation light properties to test that expectation.

II. EXPERIMENTAL DESIGN

This investigation took place in the liquid argon dewar facility "TallBo" at the Proton Assembly Building (PAB) at Fermi National Accelerator Laboratory (FNAL) from March 6 through March 20, 2014.

The experimental apparatus consisted of a prototype LBNE photon detector (PD) module immersed in LAr, prototype LBNE readout electronics, and hodoscope trigger paddles. A PD module is made up of 4 light guides that capture, waveshift, and channel VUV photons to silicon photomultipliers (SiPMs) at one end. There are 3 SiPMs per light guide, and as a consequence there are 12 channels of prototype LBNE readout electronics. Hodoscope paddles were placed on either side of the dewar and used a coincidence trigger to guarantee that the events read out passed through the dewar.

The experimental setup is described more fully below.

A. Light Guides

A schematic drawing of a cast acrylic light guide with its photosensors is shown in Fig. 1. The light guides are made from cast acrylic bars of dimensions 50.8 cm × 2.54 cm × 0.6 cm that have wavelength shifter embedded in them. The concept is described in Ref. [5]. The wavelength shifter converts VUV scintillation photons striking it to 430 nm photons inside the bar, with an efficiency of ∼50% of converting a VUV to an optical photon [6]. A fraction of the waveshifted optical photons are internally reflected to the bar's end where they are detected by SiPMs whose QE is well matched to the 430 nm waveshifted photons. The light guides were made with one of two wavelength shifters: the conventional TPB (1,1,4,4-tetraphenyl-1,3-butadiene) and the less expensive alternative bis-MSB (1,4-bis-(o-methyl-styryl)-benzene). Preliminary studies with a VUV monochromator show that the two wavelength shifters compare favorably in their waveshifting efficiency [7]. A testing program is currently underway to compare their relative performance in LAr.

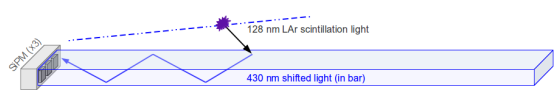

FIG. 1: Schematic drawing of a cast acrylic light guide with its photosensors. The bars have embedded wavelength shifter (WLS), either TPB or bis-MSB. Three SiPMs collect the waveshifted photons that have been internally reflected to the bar's end.

The 4 light guides in the PD module were all made with different technologies or similar technologies but different wavelength shifters. The light guide technologies and wavelength shifters used with them are listed in Table I.

TABLE I: Light guide technologies in PD module.

Label	Light Guide Technology	WLS
(a)	acrylic, flash heated	TPB
(b)	acrylic, flash heated	bis-MSB
(c)	acrylic, dipped-coated	TPB
(d)	acrylic, cast with WLS	TPB

(a, b) Two light guides were made using a similar technology but different wavelength shifters. They were both made by a "flash heating" technology; one was made with TPB and the other with bis-MSB. Both light guides were made from commercially available Lucite-UTRAN cast UVT acrylic sheet that was laser-cut into bars of the proper size. Lucite-UTRAN has the longest attenuation length of the acrylics tested [8]. For the acrylic bars to act as light guides, the waveshifted light must be generated within the volume of the acrylic. To embed the WLS in the light guide, either TPB or bis-MSB was first dissolved in methylene chloride (CH_2Cl_2). This mixture was then spray-painted from a pressurized vessel onto the plastic bars using a computer-controlled spray-paint head. What remains after the methylene chloride evaporates is a fine powder of WLS on the light guide surface. To embed the WLS in the acrylic, the coated bars are flash heated to rapidly melt the WLS into a thin outer layer of the bar without melting its center, which would lead to surface distortions [8]. The more surface distortions there are in the bar, the less effective it is as an adiabatic light guide.

(c) A dip-coating process of applying WLS solution to the acrylic bar surface was developed at MIT as an alternative to hand-painting [9]. This process improves the clarity and uniformity of the coating, as well as its scalability to the manufacture of the large number of light guides needed for LBNE. In this process the bars are first annealed for 3 hours at 230 F, after which the temperature is stepped down in 10 F increments to 120 F. The bars are then allowed to cool to room temperature. After this process is complete, the bars are wiped down on all surfaces with ethanol. Next, a solution is mixed with 1 part TPB to 2 parts UVT acrylic in toluene. This mixture is allowed to stand for 24 hours to allow the WLS and acrylic to dissolve fully, after which ethanol is added as a surfactant. Each acrylic bar is submerged in this solution for 5 minutes, removed, and then hung and left to air dry.

(d) The fourth light guide was cut from a sheet of acrylic cast with TPB mixed into the plastic. This sheet was

manufactured commercially by Astra Products, Baldwin, NY. The sheet had 1% TPB by mass added during their proprietary casting process, which distributes TPB throughout the volume. Since VUV photons have a very short penetration depth in acrylic, this manufacturing method uses far more WLS than necessary. (The penetration depth of 128 nm photons in polystyrene is < 100 nm, as estimated from Ref. [10]. The assumption made here is that polystyrene and acrylic have similar opacity in the VUV.) On the other hand, light guides function more efficiently when their surfaces are flat and the casting process results in very flat surfaces, which is a mitigating factor if the prime consideration is efficiency for the detection of VUV photons.

Which technology and wavelength shifter combination produces the most efficient light guides has been the subject of detailed tests of prototypes in LAr at TallBo. These studies will be the subject of another paper. The results reported here do not depend on the relative efficiency of the light guides.

B. Photodetectors and Photodetector Readout

At the end of each light guide are 3 SensL MicroFB-60035-SMT SiPMs [11], as shown in Fig. 1. Each SiPM has an active area of 6×6 mm^2. They are made up of an array of 18,960 microcell photodiodes, each of which is 35 μm on a side, and the microcell filling factor on the chip is 64%. The SiPMs are reverse-biased at 24.5 V.

The operating characteristics of these SiPMs have been determined by the manufacturer down to 230 K [11]. For operation in LAr, the SiPMs need to be characterized at 87 K. Since these measurements require SiPM dark spectra, the SiPMs were read out while immersed in liquid nitrogen (LN2). The dark measurements were made in LN2 rather than LAr because LN2 does not scintillate, so no systematics are introduced by scintillation light from cosmic rays or radioactive impurities. The 10 K difference in temperature between LAr and LN2 is not expected to impact the results.

Signals are processed by an SiPM Signal Processor (SSP) module that was designed and built by the HEP Electronics Group at Argonne National Laboratory (ANL) for the LBNE photon detection system. An SSP has 12 readout channels, each of which consists of a differential voltage amplifier and a 14-bit, 150 MSPS ADC that digitizes the signals with negligible dead time. The ADC has a full-scale dynamic range of 2 V, corresponding to approximately 1000 photoelectrons (pe's) at a typical SiPM gain of 3×10^6. The amplifier input impedance is 100 Ω with an overall digitizer gain of 1850 V/A. Each ADC count is equivalent to $2\text{V}/2^{14} \times (18.5\ V/V)^{-1} = 6.60 \times 10^{-3}$ mV. The SSP was designed to resolve single pe pulses and achieves a resolution of 18% FWHM.

An FPGA in the SSP implements an independent data processor for each channel. The processing includes a leading edge discriminator to detect events, amplitude analysis algorithms for measuring the peak and the integral of the waveform, a pulse pileup detection algorithm, and a constant fraction discriminator. Each digitized waveform consists of 1200 samples; the bin width of each sample is 6.67 ns and the total waveform is 8 μs long.

Fig. 2 shows dark spectra accumulated over 300 s with the SSP for one instance of a SensL MicroFB-60035-SMT SiPM in LN2. The SiPM was biased at 24.5 V. The prompt amplitude histogram shows the signals in

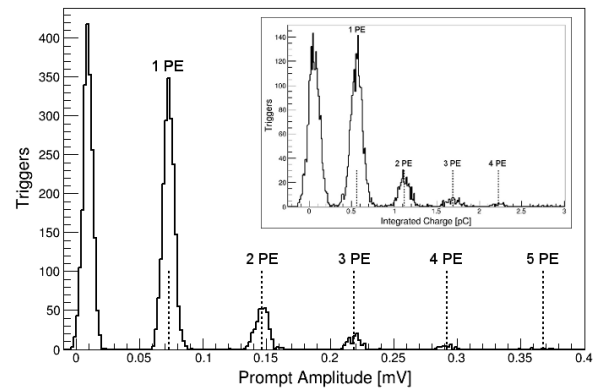

FIG. 2: Dark spectra for the prompt signal and the integrated signal (*inset*) for a SensL MicroFB-60035-SMT SiPM in LN2. The prompt amplitude is the average signal in the first 133 ns of the waveform. The integrated signal has been calibrated to charge in pC. The excellent single-pe resolution and the linearity of the response are apparent.

the first 133 ns (20 bins) of the waveforms for the dark events. The inset histogram gives the integrated charge in the waveforms over their full range. Both histograms show the excellent single-microcell resolution and the linearity of the response for this SiPM. The total charge in each waveform is determined by first summing the waveform amplitude (in ADC counts) over the N 6.67 ns time bins in the waveform, where a typical $N \approx 580$ samples includes the trigger signal and any time-correlated after-pulses that may occur. The integrated charge collected in the waveform is then calculated by converting this sum (s) to charge (c), where c [pC] $= s \times (6.60 \times 10^{-6}$ [V/ADC count]$)/100\,\Omega \times (6.67 \times 10^{-9}$ s).

The gains for the 5 SensL SiPMs were determined by dividing the mean charge in the 1 pe peak of their dark spectra by the charge of an electron. For the SiPM biased at 24.5 V shown in Fig. 2, the gain is 3.5×10^6. The mean gain for the 5 SiPMs biased at 24.5 V is $(3.54 \pm 0.05) \times 10^6$. The gain measurements were repeated for the 5 SiPMs at bias voltages in the range 23.5 – 26.5 V in steps of 0.5 V. In this range, the mean gain for the SiPMs was found to rise linearly from 2.6×10^6 at 23.5 V to 5.4×10^6 at 26.5 V.

The dark noise rates for the SiPMs were determined from their dark spectra by summing the number of triggers with prompt amplitudes ≥ 0.5 pe and dividing the sum by the 300 s data acquisition time. For the SiPM in Fig. 2, the noise rate is 7.8 Hz. The mean dark rate

for all 5 SiPMs biased at 24.5 V is 8.9 ± 1.6 Hz. For bias voltages in the range 23.5 – 24.5 V, the mean noise rate rises slowly from 4.5 – 9 Hz. For bias voltages greater than 24.5 V the noise rises more rapidly, from 13 Hz at 25 V to ∼40 Hz at 26.5 V.

For this experiment, the SiPMs were biased at 24.5 V, where the gain is high but before the noise rate has begun its rapid rise. This bias voltage is approximately 3.5 V above the breakdown voltage, $V_{br} \sim 21$ V, determined in two ways. First, the gain as a function of bias voltage was projected back to zero gain using a linear fit. Second, the SiPM was immersed in LN2 and read out by a picoammeter as the bias voltage was increased from 1 mV to 27 V. The bias voltage at which the signal began to increase exponentially was identified as V_{br}. Both methods gave consistent results.

C. The TallBo Dewar Facility

TallBo is a 460 liter dewar located at the PAB at FNAL. It is 2.13 m tall and has an inner diameter of 62.9 cm. Its large size accommodates 16 light guides in four custom PD paddle mounts designed and built at Colorado State University. Each mount supports four light guides and twelve SiPMs. A frame holding the four PD modules was hung from the lid of the dewar. The sketch on the left in Fig. 3 shows the positions of the four PD modules mounted in their frame inside TallBo. The photograph on the right shows the stainless steel TallBo dewar in PAB. Only one SSP module (12 channels = 1 PD module) was available for this experiment. The PD module read out by the SSP is shown highlighted.

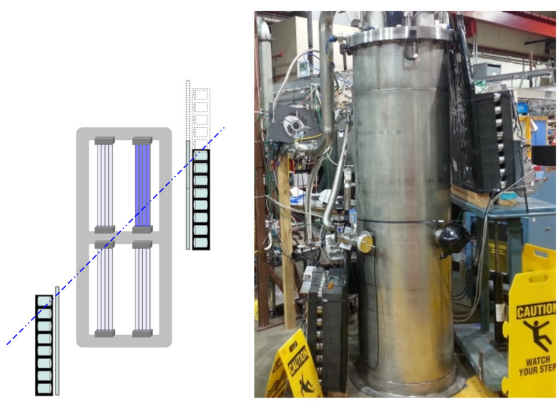

FIG. 3: *Left:* A drawing showing the 4 PD modules in the TallBo dewar and the hodoscope trigger paddles on the outside. The PD module used in this analysis is highlighted. *Right:* Photograph of TallBo dewar with hodoscope modules.

To prepare for a run, the dewar was first evacuated by a turbo pump to help reduce contamination from residual gasses and was then back-filled with gaseous argon. The gaseous argon was next replaced with ultra-high-purity (UHP) LAr that had been passed through a molecular sieve and copper filter to further remove contaminants. The most harmful contaminants to the detection of scintillation light in LAr are O_2 at the 100 parts-per-billion level [12] and N_2 at the few parts-per-million level [4, 13]. These contaminants can both quench scintillation light and affect the argon transparency at 128 nm [4]. After filling TallBo with LAr, gas from the ullage was sampled and passed through an oxygen monitor and a nitrogen monitor. The oxygen monitor reported 67 ppb in the ullage, corresponding to 74 ppb in the liquid. O_2 contamination therefore does not affect our results. The nitrogen monitor was not working properly; however, the LAr used in this experiment was supplied by AirProducts and was delivered from the same Fermilab stock used by the MicroBooNE experiment. Measurements by MicroBooNE of their LAr show the N_2 contamination to be typically < 0.4 ppm (B. Rebel, private communication). The LAr delivered to TallBo for this experiment is assumed to have had typical concentrations of contaminants and N_2 had no significant impact on the results.

Once filling was complete, the vessel was sealed and subsequently maintained at a positive internal pressure of 10 psig to ensure no additional contamination during operation. A liquid-argon condenser on TallBo reliquified gas from the ullage and returned it to the dewar, in order to maintain a constant liquid level inside.

D. Hodoscope Paddles and Trigger

Two hodoscope modules were installed on opposite sides of the TallBo dewar to select single-track cosmic-ray muons passing through the LAr volume. These hodoscope modules were loaned from the CREST balloon-based cosmic ray experiment [14]. Each module consists of 64 2-inch diameter barium-fluoride crystals, coated with TPB and arranged in an 8×8 array. Each crystal is monitored by a PMT.

Since the hodoscope modules were designed to detect bremsstrahlung photons from high-energy electrons bending in the Earth's magnetic field, they are very sensitive to extraneous photon activity around our experiment. To reject these γ showers, a pair of plastic scintillator panels covering the entire face of a hodoscope module were placed between each hodoscope module and the TallBo dewar. These panels were individually read out by PMTs. The SSP readout was then triggered by four-fold coincidence logic that required at least one hit in both hodoscope modules as well as one hit in their adjacent scintillator planes. This trigger guarantees that each event contains at least one charged particle passing through the liquid argon. Events were further filtered offline to reject showers by requiring one and only one hit in each hodoscope module. For this experiment the upper hodoscope module was positioned 1.2 m above the ground, as shown in Fig. 3.

E. SiPM Response to Scintillation Light

The objective of this investigation is to characterize the relative fraction of early light to late light for minimum ionizing cosmic-ray muons. Fig. 4 shows an example of a full 8 μs waveform from the scintillation light generated by a single-track muon in LAr selected by the hodoscope trigger in TallBo. The start time of the event

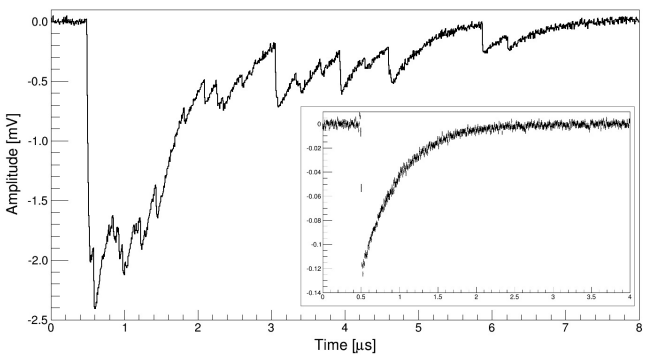

FIG. 4: An example waveform from scintillation light generated by a single-track muon in LAr selected by the hodoscope trigger in TallBo, recorded by SiPM (a)-1. The early light multi-pe pulses and the subsequent few-pe pulses are sums of single-pe pulses convolved with the SiPM's single-microcell response function. *inset:* Average single-microcell response for a SensL MicroFB-60035-SMT SiPM in LAr.

(t_0) is the arrival time of the leading edge of the early-light photons. The event can be summarized as a series of photon-initiated avalanches in the SiPM microcells, with an early many-pe pulse from the decay of the Ar_2^* singlet state followed later by single- and few-pe pulses from the decay of the Ar_2^* triplet state. The brightest events recorded correspond to only a few hundred prompt pe's detected at the SiPM, meaning multi-pe pulses represent a sum of single-pe pulses on different microcells that fall within the same 6.67 ns time bin of the waveform readout. With this assumption, a waveform represents simple sums of single-pe pulses (and associated electronics noise) convolved with the SiPM's single-microcell response function. In Fig. 4, for example, the large leading edge is the sum of approximately 20 single-pe pulses from the singlet decay, followed by a number of smaller pulses from the triplet decay.

The average single-microcell response of a SensL MicroFB-60035-SMT SiPM in LAr is shown in the inset of Fig. 4. This response was determined for each SiPM in the PD module by selecting events corresponding to 1 pe as measured by both the prompt amplitude and integrated charge. As an example, Fig. 5 shows the amplitude distributions for all single-track events on SiPM (a)-1. The prompt amplitude histogram in Fig. 5 shows the signals in the first 133 ns (20 bins) of the waveforms. The inset histogram gives the summed charge in the waveforms over the ~7.5 μs beginning at the prompt

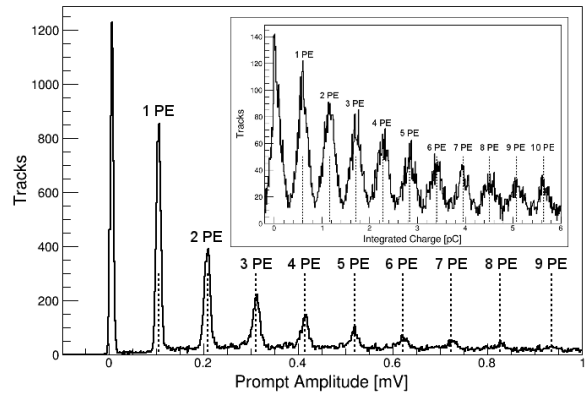

FIG. 5: Spectra for the prompt signal and the integrated signal (*inset*) for all single track triggers on SiPM (a)-1. The waveform in Fig. 4 is from this dataset. The prompt amplitude is the average signal in the first 133 ns of the waveform. The summed signal in the full waveform (8 μs) has been calibrated to charge.

rising edge. The integrated ADC counts were calibrated to charge as described previously for the dark spectra. Waveforms from cosmic-ray muons, however, are typically longer than dark waveforms (~1125 samples, or 7.5 μs) and they exhibit considerably more scintillation light in the total waveform than in the prompt signal alone.

To determine the single-microcell response function for an SiPM, all of the waveforms found to be in both 1 pe peaks were summed. The assumption is that a waveform found in the 1 pe peak of both histograms is a single pe hit on a single microcell. To improve the selection it is restricted to events in a window between 0.85 and 1.15 pe. Dividing by the number of waveforms used to calculate the sum gives the mean response for this SiPM. This mean waveform was next fit to determine the single-microcell response function, parametrized as

$$\mathcal{R}_{\mu c}(t) = A_{\mu c}\, \mathcal{E}(t; \tau, w, t_m), \tag{2}$$

where $A_{\mu c}$ is a normalization constant and $\mathcal{E}$ is the exponentially-modified Gaussian probability density function (EMG). The EMG is the convolution of the Gaussian and exponential probability density functions [15],

$$\mathcal{E}(t; \tau, w, t_m) = \frac{1}{\tau} \times \exp\left[\frac{1}{2}\left(\frac{w}{\tau}\right)^2 - \left(\frac{t - t_m}{\tau}\right)\right] \times \frac{1}{2}\left[1 + \mathrm{erf}\left(\frac{z}{\sqrt{2}}\right)\right], \tag{3}$$

where

$$z = \left(\frac{t - t_m}{w} - \frac{w}{\tau}\right).$$

Here τ is the parameter that characterizes the exponential falloff from the peak of the response, w is the width

of the Gaussian, and t_m is the mean of the Gaussian. The fit parameters for all 12 SiPMs are given in Table II.

TABLE II: Parameters in the fits to the mean single-microcell response function $\mathcal{R}_{\mu c}$ for the 12 SiPMs in the PD module.

SiPM	$A_{\mu c}$ (μV·ns)	τ (ns)	w (ns)	t_m (ns)	$\chi^2/N_{\rm DF}$
(a)-1	-58.9 ± 0.2	469.9 ± 3.4	4.4 ± 0.8	4.0 ± 0.4	1.11
(a)-2	-59.2 ± 0.2	487.6 ± 3.4	4.5 ± 0.7	4.0 ± 0.4	1.21
(a)-3	-58.9 ± 0.3	502.4 ± 4.3	4.7 ± 0.9	3.3 ± 0.5	1.49
(b)-1	-61.2 ± 0.2	467.9 ± 3.1	4.6 ± 0.7	3.6 ± 0.4	1.59
(b)-2	-58.5 ± 0.2	512.1 ± 3.2	3.6 ± 1.0	3.7 ± 0.4	1.59
(b)-3	-57.5 ± 0.2	524.6 ± 3.2	4.3 ± 0.8	3.6 ± 0.4	1.49
(c)-1	-60.9 ± 0.3	531.8 ± 4.9	4.5 ± 1.0	3.4 ± 0.5	1.15
(c)-2	-59.7 ± 0.3	520.0 ± 4.5	4.5 ± 0.9	3.7 ± 0.5	1.19
(c)-3	-58.7 ± 0.3	477.0 ± 3.7	5.1 ± 0.8	2.9 ± 0.5	1.18
(d)-1	-59.0 ± 0.2	478.0 ± 2.5	4.3 ± 0.7	3.3 ± 0.3	1.17
(d)-2	-60.1 ± 0.2	476.8 ± 2.1	4.1 ± 0.6	3.9 ± 0.3	2.12
(d)-3	-60.0 ± 0.2	469.5 ± 2.2	4.6 ± 0.5	3.8 ± 0.3	2.10

The fast rise time ($w, t_m \approx 4$ ns) is typical of both SiPMs and PMTs, and provides good timing for the trigger pulse from the fast light. The long exponential tail, however, characterized by $\tau \sim 470 - 530$ ns, is significantly longer than a PMT. This feature of an SiPM is due in part to its much larger capacitance. However, its explanation is more complicated at LAr temperatures. The expected RC time constant for this SiPM is 340 ns (100 Ω $\times$ 3400 pF [11] at room temperature); this is the decay time measured at room temperature in our lab. Among the possible causes for the longer exponential tail in LAr are additional capacitance added by the shielded twisted pair readout cable, an increase in the SiPM capacitance at LAr temperatures, and added resistance due to mechanical issues with the spring-loaded electrical connections to the SiPMs.

F. Cross Talk and After-Pulsing

To deconvolve the photodetector response from the waveforms, the single microcell response function $\mathcal{R}_{\mu c}$ needs to be modified to include effects from cross talk and after-pulsing. With these modifications, $\mathcal{R}_{\mu c}$ becomes the single pe response function, F_{pe}. Cross talk events are generated by visible light photons emitted during an avalanche that reach a neighboring pixel and induce an additional avalanche. These are prompt signals occurring in coincidence with a microcell avalanche induced by a signal photon. After-pulses are generated when electrons produced in an avalanche get trapped and are only released again after some delay, ranging from nanoseconds potentially up to several microseconds [16]. These are signals with a definite time structure. Since neither of these sources of electronics noise can be separated from the signal induced by the initial photon incident on the SiPM, their effects must be included in a model of the single pe response.

The effect of cross talk is to add a prompt second pe to the incident photon some fraction of the time. This modifies $\mathcal{R}_{\mu c}(t)$ by the factor $(1 + p_{ct})$, where p_{ct} is the probability of the emission of an additional cross talk pe. The effect of after-pulsing is to introduce an additional pe with a time structure given by the convolution $\mathcal{P}_{ap}(t) * \mathcal{R}_{\mu c}(t)$, where the probability distribution for after-pulsing has the form [16]

$$\mathcal{P}_{ap}(t) = \frac{p_{ap}}{\tau_{ap}} \exp\left(-t/\tau_{ap}\right) \qquad t \geq 0 \tag{4}$$

and $\mathcal{P}_{ap} = 0$ for $t < 0$. The single-pe response function, F_{pe}, is then

$$F_{pe}(t) = (1 + p_{ct})\mathcal{R}_{\mu c}(t) + \mathcal{P}_{ap}(t) * \mathcal{R}_{\mu c}(t). \tag{5}$$

The values for p_{ct}, p_{ap}, and τ_{ap} were determined with dark spectra like those in Fig. 2 with the SiPMs in LN2. The methods used were modifications of those described in Ref. [16]. The ratio of the number of triggers with an integrated amplitude > 1.5 pe to the number of triggers > 0.5 pe gives the probability of an extra hit due to electronics noise from either cross talk or after-pulsing. The probability of a second dark noise event within the readout window is negligible. The mean ratio for all 5 SiPMs biased at 24.5 V is 0.20 ± 0.02.

The cross talk and after-pulsing parameters were simultaneously determined by fitting the arrival time distribution of the dark noise pulses ($\mathcal{D}^k(t_i)$ for SiPM k) with a two-component function that adds a narrow Gaussian function for the cross-talk to an EMG function for the after-pulsing. The cross talk and after-pulsing parameters are determined from these fits. The arrival time distribution $\mathcal{D}^k(t_i)$ for the dark hits was deconvolved from the average waveforms using the same method described in § III A below for the single track waveforms from cosmic-ray muons. At a bias voltage of 24.5 V, the mean dark noise parameters for the 5 SiPMs are $p_{ct} = (0.18 \pm 0.02)$, $p_{ap} = (0.022 \pm 0.006)$, and $\tau_{ap} = 23 \pm 6$ ns. As the bias voltage increases to 26.5 V, p_{ct} increases to 0.24, p_{ap} nearly doubles to 0.04, and τ_{ap} remains approximately constant.

III. RESULTS

The signal detected by each SiPM represents a convolution of the SiPM's single-PE response function with the time-dependent profile of incident photons. To measure the structure of the scintillation signal due to minimum ionizing cosmic-ray muons, all waveforms with $\geq$0.5 pe prompt amplitude from single-track events passing the four-fold coincidence and offline single-track selections described in § II D were selected to define the average waveform detected by each SiPM. Between 23,177 and 28,934 such cosmic-ray muons contributed to the average waveform for each SiPM. These average waveforms

are then deconvolved using the corresponding single-PE response function defined in Eq. (5). Each deconvolved waveform represents the time-resolved structure of the signal incident on the SiPM and contains components due to UV emission from the singlet and triplet state Ar_2^* dimer. To capture the sharp rise and exponential tail of the scintillation components, these deconvolved waveforms are fit by a set of exponentially modified Gaussian functions.

A. Analysis Procedures

Let $w_j^k(t_i)$ be the amplitude of the j-th waveform in time bin t_i from a single track event in SiPM k. Fig. 4 shows one instance of $w_j^k(t_i)$ vs t_i and Fig. 5 is derived from all N waveforms $w_j^k(t_i)$ in SiPM k = (a)-1. The mean of the N pedestal-subtracted waveforms $\langle w^k(t_i)\rangle$ is given by

$$\langle w^k(t_i)\rangle = \sum_{j=1}^{N} w_j^k(t_i)/N. \tag{6}$$

Since each single or multi-pe pulse is the sum of single-pe hits on multiple microcells, the mean waveform for each SiPM is the convolution of the SiPM's single-pe response function with the time-dependent illumination profile of incident scintillation photons, $\mathcal{I}^k(t_i)$,

$$\langle w^k(t_i)\rangle = F_{pe}(t) * \mathcal{I}^k(t_i). \tag{7}$$

The Gold deconvolution algorithm implemented in the ROOT TSpectrum class was used to obtain the 12 time-dependent profiles of incident scintillation photons $\mathcal{I}^k(t_i)$. Fig. 6 shows in gray scale (main) and crosses (inset) the deconvolved $\mathcal{I}^k(t_i)$ for all single track waveforms recorded by SiPM (a)-1. Since the $\mathcal{I}^k(t_i)$ are independent of the SiPM response, the three deconvolved scintillation photon profiles from each light guide were summed to improve statistical precision. The model fits were preformed on the sums $\mathcal{I}^{(a)}(t_i)$, $\mathcal{I}^{(b)}(t_i)$, $\mathcal{I}^{(c)}(t_i)$, and $\mathcal{I}^{(d)}(t_i)$.

B. Two-Component Model

The de-excitation of the Ar_2^* dimer has two decay components with different lifetimes, a fast decay from the singlet state and a slower decay from the triplet state. The simplest model for the illumination functions $\mathcal{I}^{(a)}(t_i), \ldots$ is therefore one with two components. The character of the deconvolved profiles, like the one shown in Fig. 6, suggests fit functions of the form

$$\mathcal{I}_2(t) = A_{\rm T}\ \mathcal{E}\left(t;\tau_{\rm T}, w, t_m\right) + A_{\rm S}\ \mathcal{E}(t;\tau_{\rm S}, w, t_m), \tag{8}$$

where $\mathcal{E}$ is the EMG function, Eq. (3). The fits were carried out using the MINUIT tool in ROOT to perform a binned weighted likelihood minimization. There were

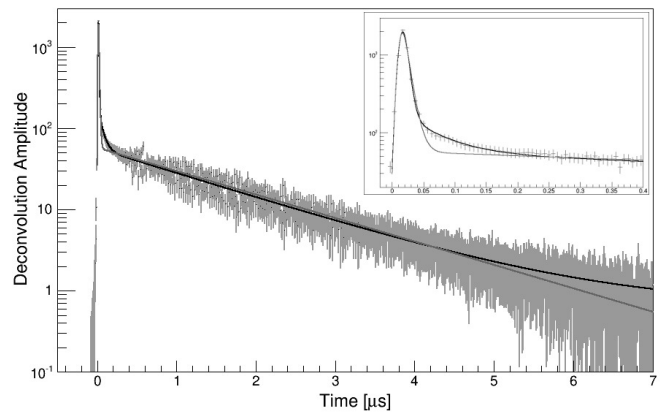

FIG. 6: The deconvolved time-dependent profile of incident scintillation photons $\mathcal{I}^k(t_i)$ for all single track waveforms recorded by SiPM k=(a)-1. $\mathcal{I}^k(t_i)$ is shown for the full waveform in gray scale and as crosses for the first 400 ns in the inset. Two- and four-component models are superimposed on $\mathcal{I}^k(t_i)$ as light and dark lines, respectively. The inset highlights the improvement to the fit in the range 50-150 ns with the addition of the intermediate component in Eq. (9).

6 parameters in the fits, $A_{\rm S}, \tau_{\rm S}, A_{\rm T}, \tau_{\rm T}, w, t_m$; w and t_m were constrained to have the same values in both components. The results of this two-component fit for the four light guides are given in Table III. Statistical errors are assigned by the fitter.

TABLE III: Fit results for the two-component model $\mathcal{I}_2(t)$ for the 4 light guides. The uncertainties are statistical.

	$\mathcal{I}^{(a)}$	$\mathcal{I}^{(b)}$	$\mathcal{I}^{(c)}$	$\mathcal{I}^{(d)}$
$A_{\rm S}$	103.1 ± 0.9	89.2 ± 0.8	146.2 ± 1.0	84.1 ± 0.8
$\tau_{\rm S}$ (ns)	8.2 ± 0.2	8.7 ± 0.2	8.5 ± 0.2	7.8 ± 0.2
$A_{\rm T}$	262.5 ± 1.4	217.0 ± 1.2	373.0 ± 1.6	130.5 ± 1.0
$\tau_{\rm T}$ (μs)	1.51 ± 0.01	1.70 ± 0.01	1.37 ± 0.01	1.65 ± 0.01
w (ns)	4.49 ± 0.09	4.53 ± 0.11	4.66 ± 0.07	4.34 ± 0.09
t_m (ns)	11.6 ± 0.1	9.0 ± 0.1	12.1 ± 0.1	11.9 ± 0.1
$\chi^2/N_{\rm DF}$	1.35	1.15	0.99	1.08

Although they have values for $\chi^2/N_{\rm DF}$ that are acceptable, the fits nevertheless still have two significant problems. Most important, the fits significantly underestimate the illumination functions in the range $50-150$ ns. This is illustrated in the inset of Fig. 6 for SiPM (a)-1. This shortcoming suggests there needs to be an additional component added to the two-component model with a mean lifetime in that range. This intermediate LAr signal component has also been reported in several previous studies [1, 2, 13, 17]. It is unclear whether this component is the result of a physics process or is instrumental in origin.

A second problem with the two-component fits is the inconsistency of the triplet state decay time constant $\tau_{\rm T}$ for the four light guides. This constant characterizes

a property of scintillation light emission in LAr and it should not depend on the technology used to detect it.

C. Four-Component Model

An improved fit model includes a contribution to describe the intermediate signal. It also includes a constant term to account for the very late light signal > 5 μs in the illumination function that does not fall away exponentially with $\tau_{\rm T}$. This component could represent an additional contribution with a mean lifetime $\tau \gtrsim \mathcal{O}(10\mu\text{s})$. The fit function for this model is given by

$$\mathcal{I}_4(t) = A_{\rm T}\,\mathcal{E}(t;\tau_{\rm T},w,t_m) + A_{\rm S}\,\mathcal{E}(t;\tau_{\rm S},w,t_m) + A_{\rm I}\,\mathcal{E}(t;\tau_{\rm I},w,t_m) + C. \quad (9)$$

Again, the fits were performed using MINUIT in ROOT. There were 9 parameters in these fits, $A_{\rm S}, \tau_{\rm S}, A_{\rm I}, \tau_{\rm I}, A_{\rm T}, \tau_{\rm T}, C, w, t_m$; w and t_m were constrained to have the same values in all three EMG components. The results of the fit to $\mathcal{I}^k(t_i)$ for all single track waveforms on SiPM (a)-1 is shown in Fig.6. The inset graphically shows the improvement to the fit with the addition of an intermediate component at $\tau_{\rm I} \approx 60$ ns.

TABLE IV: Fit results for the four-component model $\mathcal{I}_4(t)$ for the 4 light guides. The uncertainties are statistical.

	$\mathcal{I}^{(a)}$	$\mathcal{I}^{(b)}$	$\mathcal{I}^{(c)}$	$\mathcal{I}^{(d)}$
$A_{\rm S}$	91.1 ± 2.5	79.7 ± 2.4	129.6 ± 3.6	76.5 ± 1.9
$\tau_{\rm S}$ (ns)	5.0 ± 0.6	5.4 ± 0.8	5.3 ± 0.6	5.2 ± 0.5
$A_{\rm I}$	21.0 ± 1.5	17.2 ± 1.2	30.3 ± 2.1	13.2 ± 1.1
$\tau_{\rm I}$ (ns)	54 ± 13	62 ± 17	56 ± 13	57 ± 15
$A_{\rm T}$	238.4 ± 2.3	185.2 ± 2.4	352.8 ± 2.6	110.3 ± 1.7
$\tau_{\rm T}$ (μs)	1.42 ± 0.03	1.47 ± 0.04	1.38 ± 0.02	1.43 ± 0.05
C	2.05 ± 0.30	3.18 ± 0.35	0.93 ± 0.30	1.93 ± 0.24
w (ns)	5.07 ± 0.17	5.23 ± 0.22	5.22 ± 0.15	4.81 ± 0.15
t_m (ns)	13.0 ± 0.4	10.5 ± 0.4	13.4 ± 0.3	13.1 ± 0.3
$\chi^2/N_{\rm DF}$	0.66	0.41	0.32	0.48

The results of the four-component fit for the four light guides are given in Table IV. Statistical errors are assigned by the fitter. Fig. 7 shows the deconvolved scintillation profiles $\mathcal{I}^{(a)}(t_i)$, $\mathcal{I}^{(b)}(t_i)$, $\mathcal{I}^{(c)}(t_i)$, and $\mathcal{I}^{(d)}(t_i)$ in gray scale for the four light guides with the four-component model $\mathcal{I}_4(t)$ superimposed on each.

The results given in Table IV and shown in Fig. 7 argue that the four-component models provide better representations of the illumination functions and the underlying physics than the two-component models. The $\chi^2/N_{\rm DF}$ values for the four-component models are appreciably improved over the two-component model. As illustrated in the inset of Fig. 6, this model also accurately accounts for the illumination function in the range 50 – 150 ns as intended. In addition, the triplet state decay time constants $\tau_{\rm T}$ for these models are now much more consistent with one another.

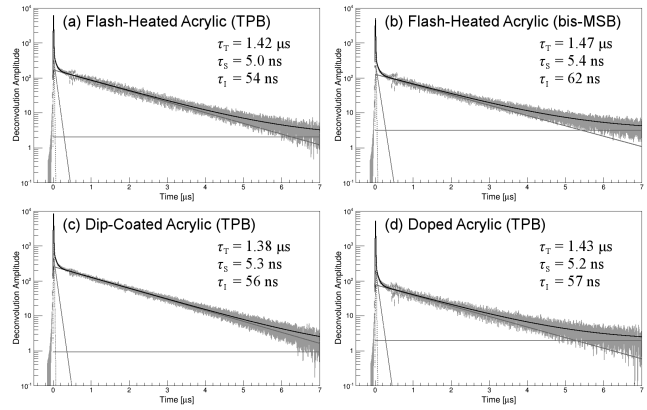

FIG. 7: The deconvolved scintillation profiles $\mathcal{I}^{(a)}(t_i)$, $\mathcal{I}^{(b)}(t_i)$, $\mathcal{I}^{(c)}(t_i)$, and $\mathcal{I}^{(d)}(t_i)$ in gray scale for the four light guides. Superimposed are the four-component fits $\mathcal{I}_4(t)$ to each. Also shown are the decay time constants for the triplet, singlet, and intermediate components.

The fits return values for the intermediate component decay time constant $\tau_{\rm I}$ in the range 54 – 62 ns for all 4 light guides. This value is similar to what was found by Ref. [17] and consistent with the feature reported in Ref. [2]. They are a factor of ∼1.5–2 longer than the decay time constants reported in Ref. [1, 13].

D. Triplet State Decay Constant and the Ratio of Singlet to Triplet Light for Cosmic Muons in LAr

Values for the parameters that characterize scintillation light from minimum ionizing muons in LAr found in § III C depend on factors whose uncertainties impact the single-pe response function F_{pe} used to deconvolve the illumination functions. These include cross talk and after-pulsing, and their uncertainties introduce systematic errors into the scintillation light parameters. In addition, the choice of the acceptance window used to select single-pe events for the determination of the average single-microcell response function $\mathcal{R}_{\mu c}$ also leads to variations in F_{pe} that introduce systematic uncertainties. Uncertainties in the waveforms themselves do not add significantly to the systematic error budget.

Systematic uncertainties on the scintillation parameters are identified by varying the cross talk and after-pulsing parameters according to the variation measured in LN2: $\Delta p_{ct} = \pm 0.02$, $\Delta p_{ap} = \pm 0.006$, and $\Delta\tau_{ap} = \pm 6$ ns. For the acceptance window around the 1-pe peak used to determine $\mathcal{R}_{\mu c}$, the upper and lower boundaries were varied by $\Delta(\text{window}) = \pm 0.05$ pe. The resulting variations of each of the scintillation fit parameters were consistently smaller than the statistical uncertainties on the central values. These variations about the central values were summed in quadrature and assigned as the systematic uncertainty to each scintillation parameter.

One important parameter characterizing the scintillation light in LAr is the triplet state decay time constant $\tau_{\rm T}$ for minimum ionizing cosmic-ray muons. Table V summarizes the results for the 4 light guides. These values all agree with one another within errors. This parameter has not previously been directly measured for cosmic-ray muons. It has however been reported for electrons, where measurements are reported in the range 1.2–1.6 μs [1, 2, 12, 13, 17, 18]. Although the mean value for $\tau_{\rm T}$ in Table V falls in the middle of this range, the e^- measurements found in the literature for the most part do not have overlapping error bars. This makes it difficult to assess whether $\tau_{\rm T}$ for muons and electrons are consistent with one another.

TABLE V: The decay time constant $\tau_{\rm T}$ from the triplet state for cosmic-ray muons in LAr from the 4-component model fit.

light guide	$\tau_{\rm T}$ (μs)	± (stat.)	± (sys.)
(a)	1.42	± 0.03	± 0.003
(b)	1.47	± 0.04	± 0.008
(c)	1.38	± 0.02	± 0.003
(d)	1.43	± 0.05	± 0.012
mean	1.43	± 0.04	± 0.007

Table VI gives another important parameter characterizing scintillation light in LAr – the fraction of singlet to triplet light for cosmic-ray muons. There are several ways to characterize this parameter. Here we use the ratio of the amplitudes of the singlet and triplet components $R = A_{\rm S}/A_{\rm T}$ from the four-component model. For alternative definitions, the parameters given for the four-component model in Table IV can be used.

TABLE VI: Amplitudes of the singlet and triplet components of scintillation light and their ratio $R = A_{\rm S}/A_{\rm T}$ for cosmic-ray muons in LAr from the 4-component model fit.

light guide	$A_{\rm S}$	± (stat.)	± (sys.)
(a)	91.1	± 2.5	± 1.2
(b)	79.7	± 2.4	± 0.9
(c)	129.6	± 3.6	± 2.4
(d)	76.5	± 1.9	± 0.9
	$A_{\rm T}$	± (stat.)	± (sys.)
(a)	238.4	± 2.3	± 1.4
(b)	185.2	± 2.4	± 0.3
(c)	352.8	± 2.6	± 1.5
(d)	110.3	± 1.7	± 0.1
	R	± (stat.)	± (sys.)
(a)	0.38	± 0.01	± 0.007
(b)	0.43	± 0.01	± 0.006
(c)	0.37	± 0.01	± 0.008
(d)	0.69	± 0.02	± 0.009

There are two important observations to be made about the results in Table VI. First, measurements of the ratio R using the 3 surface-coated bars (a), (b), and (c) are in agreement with one another, with a mean of 0.39 ± 0.01 (stat.) $\pm$ 0.008 (sys.). However, R measured by the acrylic light guide cast with wavelength shifter in its bulk volume is significantly different. One possible explanation is that some process in the bulk plastic is removing or delaying late light photons as they propagate to the SiPM. Second, there is no apparent difference in R for light guides (a) and (c) coated with TPB and light guide (b) coated with bis-MSB. This adds additional evidence [7] to support bis-MSB as a promising (and more affordable) alternative wavelength shifter to TPB for converting VUV scintillation light in LAr into the optical.

Until this study, R for minimum ionizing muons in LAr had not been measured directly. An indirect measurement, however, has been reported in Ref. [19]. To directly compare those results to R found here, it is necessary to assume that ∼100% of the triplet state light generated by cosmic muons in LAr is absorbed and then re-emitted by xenon when LAr is doped with it, and that the xenon dopant has no effect on the singlet signal. Since there is no time resolved data described in Ref. [19], there are many possible ways to interpret the indirect measurement of 0.24 ± 0.08 in terms of the parameters reported in Table IV. In terms of those parameters, the measurement most likely falls between $A_{\rm S}/(A_{\rm S}+A_{\rm I}+A_{\rm T}) \approx 0.27$ and $(A_{\rm S}+A_{\rm I})/(A_{\rm S}+A_{\rm I}+A_{\rm T}) \approx 0.33$ for the 3 surface-coated bars, values that are consistent with 0.24 within the statistical errors reported. Moreover, since there are no systematic errors given, the uncertainties on the measurement in Ref. [19] are likely underestimated.

The value of R for minimum ionizing cosmic-ray muons in LAr is expected to be similar to R measured for minimum ionizing electrons in LAr. Measurements of R for electrons fall between lower values of 0.25 [13] and 0.26 [20] and an upper value of 0.30 [1]. (In Ref. [2, 17], the electrons studied were not minimum ionizing.) There are no errors given for the older, upper value of R reported in Ref. [1], so it is difficult to judge whether R found there is consistent. The value measured here is clearly not consistent with the lower values, although those measurements are also reported without uncertainties. Further measurements are required to understand whether R can be used to discriminate minimum ionizing muons from minimum ionizing electrons, as the recent measurements suggest. Still, clearly R can be used to distinguish minimum ionizing muons from more heavily ionizing α particles [1, 17, 20].

IV. CONCLUSIONS

The experiment presented in this paper has directly measured the time-resolved scintillation signal from the passage of minimum ionizing cosmic-ray muons through liquid argon. The long lifetime of the decay of the triplet state of the $\rm Ar_2^*$ dimer was measured to be $\langle\tau_{\rm T}\rangle = 1.43 \pm 0.04$ (*stat.*) $\pm$ 0.007 (*sys.*) μs. The dependence of the relative contributions from the fast and slow scintillation components on the ionization density of charged par-

ticles is valuable for pulse-shape discrimination. Whether the value of R for minimum ionizing muons found here, $R = 0.39 \pm 0.01$ (stat.) ± 0.008 (sys.), is consistent with R for minimum ionizing electrons requires further investigation. However, it clearly differs significantly from that of heavily ionizing particles such as alphas and nuclear fragments [1, 17].

The disagreement between the ratio of fast to slow light measured by light guide (d) and the others could be due to additional absorption and emission properties of TPB that contribute significantly to light propagated through acrylic doped with the wavelength shifter. The emission characteristics of dissolved TPB have been shown to depend on the viscosity of the solvent [21] and the time-resolved emission properties of TPB after excitation by the high-energy 128 nm LAr scintillation photons has not been studied. The proprietary process used to dope acrylic with TPB could also introduce new and unknown characteristics to the polymer. Further investigation of the response of TPB embedded in acrylic, both thin films and bulk, to VUV excitation is well-motivated.

The experiment has also demonstrated the functionality of the prototype photon detection system being developed for LBNE. At LAr temperatures SiPMs have excellent single-pe response with low noise. They are linear in their response. When paired with the high-resolution SSP readout electronics, SiPMs are capable of precise timing measurements. These results demonstrate the potential for such a photon detection system to provide pulse-shape discrimination to distinguish different particle species. Furthermore, this study provided the first side-by-side test comparing the response of bis-MSB and TPB to the 128 nm photons from LAr and showed that bis-MSB wavelength shifter remains as a promising alternative to TPB.

Finally, this study has demonstrated a straightforward method for determining the time-dependent profile of incident scintillation photons generated by minimum ionizing cosmic-ray muons in LAr. Although the long capacitive tail in the SiPM response could have been an obstacle to the analysis, it was not – the fast response of the SiPMs enabled high-precision timing measurements of the incident light, even before the SiPM returned to its baseline from large signals. The cross talk, after-pulsing, and dark noise characteristics of the SiPM proved to be simple to incorporate into a description of the SiPM's single-pe response central to the analysis. This experiment shows that a LAr photon detection system based on light guides and SiPMs is capable of making the detailed and precise measurements of the properties of the scintillation light needed for future large volume LAr detectors like LBNE.

V. ACKNOWLEDGMENTS

This work was partially supported by the Office of High Energy Physics of the DOE with grant DE-SC0010120 and by Brookhaven National Laboratory with grant 240296-A3. The authors wish to thank the many people who helped make this work possible. At IU: B. Adams, B. Baptista, B. Baugh, M. Gebhard, B. Howard, M. Lang, J. Musser, P. Smith, J. Urheim. At MIT: L. Bugel, J. Conrad, B. Jones, Z. Moss, M. Toups. At Fermilab: R. Davis, M. Johnson, B. Miner, S. Pordes, B. Rebel, M. Ruschman. At ANL: J. Anderson, P. DeLurgio, G. Drake, V. Guarino, A. Kreps, M. Oberling. At Colorado State: N. Buchanan, F. Craft, T. Cummings, J. Jablonski, D. Warner, R. Wasserman.

[1] A. Hitachi et al., Phys. Rev.B **27**, 5279 (1983).
[2] W. Lippincott et al., Phys.Rev.C **78**, 035801 (2008).
[3] M. Antonello et al., ICARUS-TM, 06-03 (2006).
[4] B. Jones et al., JINST **8**, P07011 (2013).
[5] L. Bugel et al., Nucl. Instrum. & Meth. **A640**, 69 (2011).
[6] V. Gehman et al., Nucl. Instrum. Meth. A **654**, 116 (2011).
[7] B. Baptista and S. Mufson, JINST **8**, C09006 (2013).
[8] S. Mufson and B. Baptista, JINST **8**, C09012 (2013).
[9] B. Baptista et al., *arxiv:1210.3793*.
[10] W. Buck, B. Thomas, and A. Weinreb, J.Chem.Phys. **48**, 549 (1968).
[11] SensLCorporation, URL `http://sensl.com/products-page/bseries/microfb-600xx-smt/`.
[12] R. Acciarri et al., JINST **5**, P05003 (2010).
[13] R. Acciarri et al., JINST **5**, P06003 (2010).
[14] S. Coutu et al., Nucl. Phys. B (Proc. Suppl.) **27**, 250 (2011).
[15] N. Gale, Nucl.Phys. **38**, 252 (1962).
[16] P. Eckert et al., Nucl. Instrum. Meth. A **620**, 217 (2010).
[17] P. Peiffer et al., JINST **3**, P08007 (2008).
[18] T. Heindl et al., EPL **91**, 62002 (2010).
[19] P. Cennini et al., NIM **A 432**, 240 (1999).
[20] G. Carvalho, M.J.and Klein, J.Luminescence **18/19**, 487 (1979).
[21] N. Dickson, Ph.D. thesis, Ohio State University (2011).